Automatica 151 (2023) 110936

Contents lists available at ScienceDirect

Automatica

journal homepage: www.elsevier.com/locate/automatica

Brief paper

Elongation of curvature-bounded path☆

Zheng Chen [a,b,*], Kun Wang [a], Heng Shi [c]

[a] School of Aeronautics and Astronautics, Zhejiang University, Hangzhou 310027, Zhejiang, China
[b] State Key Laboratory of Fluid Power and Mechatronic Systems, Hangzhou 310027, Zhejiang, China
[c] Department of Precision Instrument, Tsinghua University, Beijing 100084, China

ARTICLE INFO

Article history:
Received 19 October 2021
Received in revised form 17 November 2022
Accepted 5 February 2023
Available online 26 February 2023

Keywords:
Dubins vehicle
Curvature-bounded path
Cooperative guidance
Path elongation

ABSTRACT

The elongation of curvature-bounded paths to an expected length is fundamentally important to plan missions for nonholonomic-constrained vehicles in many practical applications, such as coordinating multiple nonholonomic-constrained vehicles to reach a destination simultaneously or performing a mission with a strict time window. In the paper, by applying the properties of the reachability set of curvature-bounded paths, the explicit conditions for the existence of curvature-bounded paths joining two oriented points with an expected length are established. These existence conditions are numerically verifiable, allowing readily checking the existence of curvature-bounded paths between two prescribed oriented points with a desired length. In addition, once the existence conditions are met, elongation strategies are provided to get curvature-bounded paths with the expected length. Finally, some examples of minimum-time path planning for multiple Dubins vehicles to cooperatively achieve a triangle-shaped formation are presented, illustrating and verifying the developments of the paper.

1. Introduction

The model of unidirectional nonholonomic vehicles, moving only forward at a constant speed with a minimum turn radius, provides a good approximation to the kinematics of many vehicles, such as fixed-wing aerial vehicles, autonomous underwater vehicles, and uninhabited ground vehicles. Following the work by Markov (1887) in 1887 and the work by Dubins (1957) in 1957, such a nonholonomic vehicle has been named Markov–Dubins vehicle (Bakolas & Tsiotras, 2013; Kaya, 2017) or simply Dubins vehicle (Boissonnat, Cérézo, & Leblond, 1994; Bui, Boissonnat, Souères, & Laumond, 1994; Meyer, Isaiah, & Shima, 2015). Since the Dubins vehicle has a minimum turn radius, the curvature of any feasible path of Dubins vehicle is bounded almost everywhere. For the sake of simplicity, we use the term of "curvature-bounded path" to denote the feasible path of a Dubins vehicle in this paper.

It is important to find curvature-bounded paths with an expected length in practical applications (Ding, Xin, & Chen, 2019). For instance, coordinating multiple Dubins vehicles from different initial states to the same final condition simultaneously requires planning curvature-bounded paths with an expected length (Shanmugavel, Tsourdos, White, & Żbikowski, 2010; Yao, Qi, Zhao, & Wan, 2017; Yao et al., 2020). Another example is that a Dubins vehicle performs a mission with a strict time window, which requires planning a curvature-bounded path with a specific length. For this reason, the issue of finding curvature-bounded paths with expected lengths has attracted extensive attention in the past decades.

In order to find a curvature-bounded path with an expected length, it is common in the literature to first find the shortest curvature-bounded path with the same boundary conditions, and then to use some elongation strategies to elongate the shortest curvature-bounded path to the expected length. When the direction of the final tangent vector is not constrained, some iterative algorithms were developed in Schumacher, Chandler, Rasmussen, and Walker (2003) to elongate curvature-bounded paths. Meyer et al. (2015) proposed three strategies to elongate curvature-bounded paths for intercepting a moving target at a given time. Recently, it was proven by Ding et al. (2019) that if the boundary conditions lie in a specific set, the shortest curvature-bounded path cannot be elongated to arbitrary length.

In all the papers cited above, the direction of the final tangent vector is considered free. If the tangent vectors at both oriented points are fixed, the shortest curvature-bounded paths are

☆ This work was supported by the National Natural Science Foundation of China (Grant Nos. 61903331 and 62088101) and 1912 project. The material in this paper was not presented at any conference. This paper was recommended for publication in revised form by Associate Editor Andrey V. Savkin under the direction of Editor Ian R. Petersen.

* Corresponding author at: School of Aeronautics and Astronautics, Zhejiang University, Hangzhou 310027, Zhejiang, China.
E-mail addresses: z-chen@zju.edu.cn (Z. Chen), wongquinn@zju.edu.cn (K. Wang), shiheng@tsinghua.edu.cn (H. Shi).

https://doi.org/10.1016/j.automatica.2023.110936
0005-1098/

composed of circular arcs and straight-line segments (Boissonnat et al., 1994; Dubins, 1957). The geometric pattern of each shortest curvature-bounded path between two oriented points is CCC, CSC, or their substrings, where "C" denotes a circular arc and "S" denotes a straight-line segment. It was proposed in Shanmugavel, Tsourdos, Zbikowski, and White (2005) to elongate the shortest curvature-bounded path between two oriented points by increasing the turning radius of circular arcs. Ortiz, Kingston, and Langbort (2013) provided path elongation strategies with a strict assumption that the shortest curvature-bounded paths are of type CSC. The Dubins paths with clothoid arcs were used in Shanmugavel et al. (2010) to generate curvature-bounded paths with expected lengths. Recently, a homotopic approach was developed by Yao, Qi, Yue, and Wan (2020) and Yao et al. (2017) to continuously elongate curvature-bounded paths.

In this work we assume that the operation of autonomous vehicles in a time-coordinated manner requires to first assign a common length (or time) to a mission planner, which then decides what paths to follow *in situ* to achieve the assigned mission. In this respect, mission planners should be able to elongate shortest curvature-bounded paths to the same expected length in real time. However, the elongation strategies cited in the previous paragraph may fail to find a curvature-bounded path with an expected length according to the homotopic and topologic approaches by Ayala (2015, 2017), Ayala and Rubinstein (2014, 2016), Yao et al. (2020) and Yao et al. (2017). In order to make sure that a mission planner is successful to plan cooperative paths in real time, one needs to first address the fundamental issue that there exists at least a curvature-bounded path with the expected length. Once a curvature-bounded path with an expected length exists, another issue is how to reliably find the curvature-bounded path in real time.

In order to establish the conditions for the existence of curvature-bounded paths with an expected length, the properties of the reachability set of Dubins vehicle constructed by Patsko, Pyatko, and Fedotov in the remarkable work (Patsko, Pyatko, & Fedotov, 2003) are employed. It is shown in Patsko et al. (2003) that the boundary of the reachability set can be reached by extremal paths of CCC, CSC, or their substrings. This allows us to establish explicit conditions for the existence of curvature-bounded paths with an expected length between two oriented points. To be specific, the space of pairs of initial/final oriented points was divided into two complementary sets: $\mathcal{O}$ and $\mathcal{O}^c$. If the space of pairs of initial/final oriented points lies in $\mathcal{O}$, the shortest curvature-bounded path can be elongated to arbitrary length (cf. Proposition 2). However, if the space of pairs of initial/final oriented points lies in $\mathcal{O}^c$, there exists an interval to which any shortest curvature-bounded path cannot be elongated (cf. Proposition 4). Once the interval exists, the explicit conditions for the boundary of the interval are presented. This allows us to assign a feasible length (or time) to the mission planner. For any feasible length, an elongation strategy is provided in the paper to elongate the shortest curvature-bounded to the feasible length. Finally, some examples of minimum-time cooperative path planning for multiple Dubins vehicles to simultaneously complete a mission is presented, illustrating and verifying the developments of the paper.

2. Definitions and notations

Denote by $T\mathbb{R}^2$ the tangent bundle of $\mathbb{R}^2$. Any element in $T\mathbb{R}^2$ corresponds to an oriented point $(\boldsymbol{x}, \boldsymbol{v})$ where $\boldsymbol{x}$ is a point in $\mathbb{R}^2$ and $\boldsymbol{v}$ is a tangent vector to $\mathbb{R}^2$ at $\boldsymbol{x}$. For notational simplicity, we also use capital letters X and Y to denote the elements in $T\mathbb{R}^2$ in this paper, and we set

$X := (\boldsymbol{x}, \boldsymbol{v})$ and $Y := (\boldsymbol{y}, \boldsymbol{w})$.

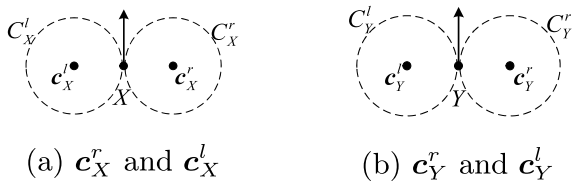

(a) $\boldsymbol{c}_X^r$ and $\boldsymbol{c}_X^l$ (b) $\boldsymbol{c}_Y^r$ and $\boldsymbol{c}_Y^l$

Fig. 1. The geometry of C_X^r, C_X^l, C_Y^r, and C_Y^l.

Definition 1 (*Curvature-Bounded Path Ayala & Rubinstein, 2016*)**.** Given any two oriented points $(\boldsymbol{x}, \boldsymbol{v})$ and $(\boldsymbol{y}, \boldsymbol{w})$ in $T\mathbb{R}^2$, a path $\gamma : [0, s] \to \mathbb{R}^2$ connecting the two oriented points is a curvature-bounded path if

- γ is C^1 and piecewise C^2;
- γ is parameterized by arc length, i.e., $\|\gamma'(t)\| = 1$ for all $t \in [0, s]$;
- $\gamma(0) = \boldsymbol{x}$, $\gamma'(0) = \boldsymbol{v}$, $\gamma(s) = \boldsymbol{y}$, and $\gamma'(s) = \boldsymbol{w}$;
- $\gamma''(t) \le \kappa$ for all $t \in [0, s]$ when defined, where $\kappa > 0$ is a constant.

Definition 2. We denote by $\Gamma(X, Y)$ the space of all the curvature-bounded paths from X to Y. And for each path $\gamma \in \Gamma(X, Y)$, we denote by $\ell(\gamma)$ the length of γ. We also denote by γ_m the shortest curvature-bounded path in $\Gamma(X, Y)$, and denote by $\ell_m > 0$ the length of γ_m, i.e., $\ell_m = \ell(\gamma_m)$.

Definition 3. For any given X and Y, a path $\gamma \in \Gamma(X, Y)$ is said to have anti-parallel tangents if there are two different points on γ so that the tangent vectors at the two points are anti-parallel.

It has been shown by Dubins (1957) that the shortest curvature-bounded path between two oriented points lies in a sufficient family of six candidates. Denote by "C" a circular arc with radius of $1/\kappa$, and denote by "S" a straight-line segment. Then, we have the following remark.

Remark 1 (*Dubins Path Dubins, 1957*)**.** The shortest curvature-bounded path in $\Gamma(X, Y)$ takes a geometric pattern of either CCC or CSC or their substrings where

- CCC = { RLR, LRL },
- CSC = { RSR, RSL, LSR, LSL}

where R (resp. L) means that the corresponding circular arc has a right-turning (resp. left-turning) direction.

Thanks to the geometric patterns in Remark 1, γ_m can be analytically computed by comparing at most 6 candidate paths; see Shkel and Lumelsky (2001).

Before proceeding, we present some useful notations. Let C_X^r and C_X^l be two tangent circles of radius $1/\kappa$, lying on the right and left side of the initial oriented point X, respectively, as shown by the two dashed circles in Fig. 1(a). We denote by $\boldsymbol{c}_X^r$ and $\boldsymbol{c}_X^l$ the centers of C_X^r and C_X^l, respectively. The same applies to C_Y^r, C_Y^l, $\boldsymbol{c}_Y^r$, and $\boldsymbol{c}_Y^l$, as shown in Fig. 1(b). Let C_η be a circular arc with a radian of $\eta \ge 0$, and denote by S_d a straight-line segment with a length of $d \ge 0$. With these new notations, when necessary we will represent CCC and CSC by $\mathrm{C}_\eta\mathrm{C}_\zeta\mathrm{C}_\xi$ and $\mathrm{C}_\eta\mathrm{S}_d\mathrm{C}_\xi$, respectively.

3. Elongation of curvature-bounded path

Before elongating a curvature-bounded path between two oriented points to an expected length, one has to ensure that there exists a curvature-bounded path between the same oriented points with the expected length. In this section, the conditions

for the existence of curvature-bounded path with an expected length will be established, and once the existence conditions are met, elongation strategies will be provided.

3.1. Elongation of CCC-path

This subsection will show how to elongate the shortest curvature-bounded path if its geometric pattern is of type CCC. Before proceeding, we first show that any curvature-bounded path with anti-parallel tangents (cf. Definition 3) can be elongated to arbitrary length by the following lemma.

Lemma 1 (*Ayala, 2017*). *If $\gamma \in \Gamma(X, Y)$ has anti-parallel tangents, then for any $s \geq \ell(\gamma)$ there exists a curvature-bounded path $\bar{\gamma} \in \Gamma(X, Y)$ so that $s = \ell(\bar{\gamma})$.*

The proof of this lemma can be found in Ayala (2017).

Proposition 1. *If γ_m in $\Gamma(X, Y)$ takes a geometric pattern of $\mathrm{C}_\eta\mathrm{C}_\zeta\mathrm{C}_\xi$, then for any $s \geq \ell_m$ there exists a $\gamma \in \Gamma(X, Y)$ such that $s = \ell(\gamma)$.*

Proof. In view of Bui et al. (1994, Lemma 3), if γ_m is of type $\mathrm{C}_\eta\mathrm{C}_\zeta\mathrm{C}_\xi$, we have that the middle circular arc is a major arc, i.e., $\zeta \in (\pi, 2\pi)$. Note that a circular arc C_ζ with $\zeta \geq \pi$ admits anti-parallel tangents. Thus, according to Lemma 1, for every $s \geq \ell_m$ there exists a $\gamma \in \Gamma(X, Y)$ so that $s = \ell(\gamma)$, completing the proof. □

Proposition 1 indicates that if the shortest curvature-bounded path is of type CCC, it can be elongated to arbitrary length without breaking the constraint on maximum curvature. In the following subsection, we shall show the elongation ability of the shortest curvature-bounded path if its geometric pattern is of type CSC.

3.2. Elongation of CSC-path

For notational simplicity, we define the following five sets.

$$\mathcal{O}_1 = \{(X, Y) \in (T\mathbb{R}^2)^2 | \gamma_m \in \mathrm{C}_\eta\mathrm{S}_d\mathrm{C}_\xi \text{ with } \eta \geq \pi\}$$
$$\mathcal{O}_2 = \{(X, Y) \in (T\mathbb{R}^2)^2 | \gamma_m \in \mathrm{C}_\eta\mathrm{S}_d\mathrm{C}_\xi \text{ with } \xi \geq \pi\}$$
$$\mathcal{O}_3 = \{(X, Y) \in (T\mathbb{R}^2)^2 | \gamma_m \in \mathrm{C}_\eta\mathrm{S}_d\mathrm{C}_\xi \text{ with } d \geq \tfrac{4}{\kappa}\}$$
$$\mathcal{O}_4 = \{(X, Y) \in (T\mathbb{R}^2)^2 | \gamma_m \in \mathrm{C}_\eta\mathrm{S}_d\mathrm{C}_\xi \text{ with } d(c_X^r, c_Y^r) \geq 4/\kappa\}$$
$$\mathcal{O}_5 = \{(X, Y) \in (T\mathbb{R}^2)^2 | \gamma_m \in \mathrm{C}_\eta\mathrm{S}_d\mathrm{C}_\xi \text{ with } d(c_X^l, c_Y^l) \geq 4/\kappa\}$$

where the function $d : \mathbb{R}^2 \times \mathbb{R}^2 \to \mathbb{R}_+$ denotes the Euclidean distance between two points. Let $\mathcal{O} \subset (T\mathbb{R}^2)^2$ be the union of $\mathcal{O}_1$, $\mathcal{O}_2$, …, $\mathcal{O}_5$, i.e.,

$$\mathcal{O} := \mathcal{O}_1 \cup \mathcal{O}_2 \cup \mathcal{O}_3 \cup \mathcal{O}_4 \cup \mathcal{O}_5,$$

and let $\mathcal{O}^c \subset (T\mathbb{R}^2)^2$ be the complementary set of $\mathcal{O}$, i.e.,

$$\mathcal{O}^c := \{(X, Y) \in (T\mathbb{R}^2)^2 | \gamma_m \in \mathrm{CSC},\ (X, Y) \notin \mathcal{O}\}.$$

In view of the definitions of $\mathcal{O}$ and $\mathcal{O}^c$, it is clear that for any $(X, Y) \in (T\mathbb{R}^2)^2$ so that the geometric pattern of γ_m is CSC, we have $(X, Y) \in \mathcal{O} \cup \mathcal{O}^c$. By the following lemmas and theorems, we shall establish the conditions for the existence of $\gamma \in \Gamma(X, Y)$ with expected lengths in the two separate sets $\mathcal{O}$ and $\mathcal{O}^c$.

Lemma 2. *Given any $\gamma \in \Gamma(X, Y)$, if it has a straight-line segment with its length not less than $4/\kappa$, then for any $s \geq \ell(\gamma)$ there exists a curvature-bounded path $\bar{\gamma} \in \Gamma(X, Y)$ so that $s = \ell(\bar{\gamma})$.*

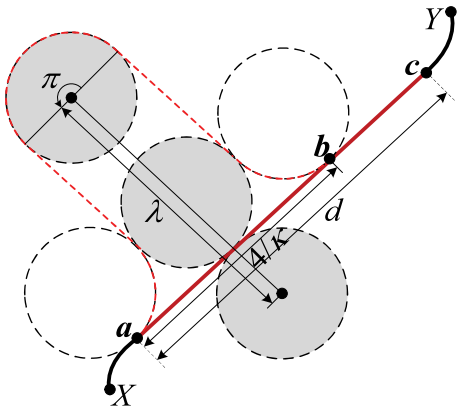

Fig. 2. Elongation of a path in $\Gamma(X, Y)$ containing a straight-line segment with its length not less than $4/\kappa$.

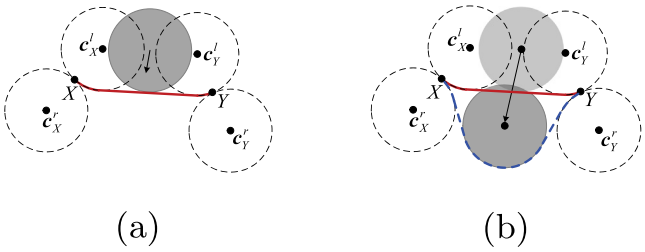

Fig. 3. An elongation strategy for γ_m with $(X, Y) \in \mathcal{O}_4$.

Proof. Denote by $d \geq 4/\kappa$ the length of the straight-line segment, as shown in Fig. 2. Denote by $\boldsymbol{a}$ and $\boldsymbol{c}$ the initial and final points of the straight-line segment. Then, we can choose a point $\boldsymbol{b}$ on the straight-line segment so that the distance between $\boldsymbol{a}$ and $\boldsymbol{b}$ is $4/\kappa$. We can use a circular disk of radius $1/\kappa$ to deform the straight-line segment from $\boldsymbol{a}$ to $\boldsymbol{b}$ without changing the tangent vectors at $\boldsymbol{a}$ and $\boldsymbol{b}$, as shown by Fig. 2. Thus, the path γ can be elongated to arbitrary length without breaking the constraint on maximum curvature, completing the proof. □

Proposition 2. *If $(X, Y) \in \mathcal{O}$, for any $s \geq \ell_m$ there exists a $\gamma \in \Gamma(X, Y)$ such that $s = \ell(\gamma)$.*

Proof. We first consider the case of $(X, Y) \in \mathcal{O}_1 \cup \mathcal{O}_2$. Note that a major circular arc has anti-parallel tangents. Thus, according to the definitions of $\mathcal{O}_1$ and $\mathcal{O}_2$, we have that γ_m has anti-parallel tangents in this case. Therefore, according to Lemma 1, γ_m can be elongated to arbitrary length. This means that, if $(X, Y) \in \mathcal{O}_1 \cup \mathcal{O}_2$, for any $s \geq \ell_m$ there exists a $\gamma \in \Gamma(X, Y)$ so that $s = \ell(\gamma)$.

From now on, we consider $(X, Y) \in \mathcal{O}_3$. In this case, there exists a straight-line segment with its length not less than $4/\kappa$ along γ_m. Thus, according to Lemma 2, γ_m can be elongated to arbitrary length, indicating that for any $s \geq \ell_m$ there exists a $\gamma \in \Gamma(X, Y)$ so that $s = \ell(\gamma)$.

Regarding the case that $(X, Y) \in \mathcal{O}_4$, as shown in Fig. 3(a), we are able to deform γ_m (red solid curve) by moving a circular disk of radius $1/\kappa$ without breaking the constraint on curvature, as shown by the blue dashed curve in Fig. 3(b). Thus, in the case of $(X, Y) \in \mathcal{O}_4$, γ_m can be elongated to arbitrary length. The same strategy can be applied to elongating γ_m if $(X, Y) \in \mathcal{O}_5$. Thus, if $(X, Y) \in \mathcal{O}_4 \cup \mathcal{O}_5$, for any $s \geq \ell_m$ there exists a $\gamma \in \Gamma(X, Y)$ so that $s = \ell(\gamma)$, completing the proof. □

As a result of Proposition 2, it is apparent that if $(X, Y) \in \mathcal{O}$, γ_m can be elongated to arbitrary length without breaking the constraint on maximum curvature.

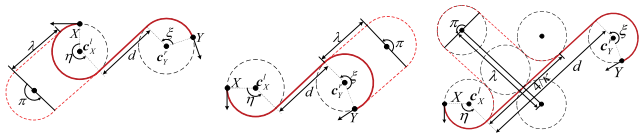

(a) $C_\eta SC$ $(\eta \geq \pi)$ (b) CSC_ξ $(\xi \geq \pi)$ (c) $CS_dC(d \geq \frac{4}{\kappa})$

Fig. 4. Elongation of γ_m with $(X, Y) \in \mathcal{O}_1 \cup \mathcal{O}_2 \cup \mathcal{O}_3$.

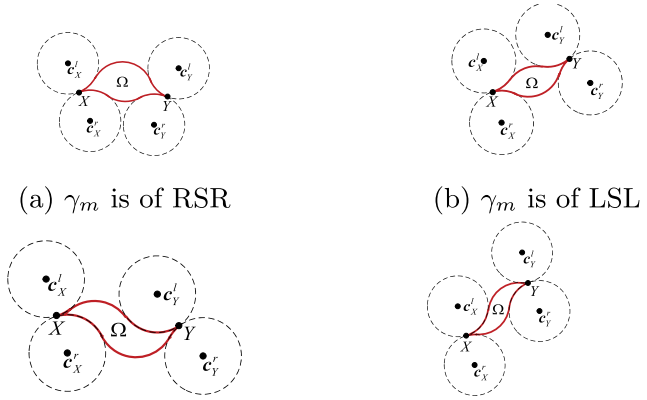

(a) γ_m is of RSR (b) γ_m is of LSL

(c) γ_m is of RSL (d) γ_m is of LSR

Fig. 5. Geometry for the closed region Ω.

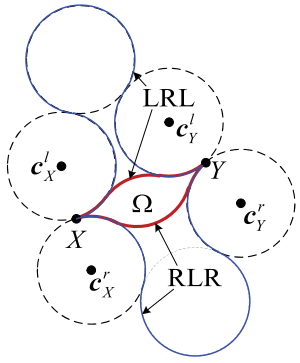

Fig. 6. Existence of two LRL-paths and two RLR-paths.

An elongation strategy for $(X, Y) \in \mathcal{O}_4 \cup \mathcal{O}_5$ has been provided by Fig. 3. Regarding the case of $(X, Y) \in \mathcal{O}_1 \cup \mathcal{O}_2 \cup \mathcal{O}_3$, an elongation strategy is illustrated in Fig. 4.

It has been shown in Ayala and Rubinstein (2014, 2016) that if $(X, Y) \in \mathcal{O}^c$ there exists a closed region Ω, as shown in Fig. 5. Once $(X, Y) \in \mathcal{O}^c$, there exist two paths of type RLR and two paths of type LRL, as shown in Fig. 6. We denote by RLR^s and RLR^l the shorter and longer RLR-paths, respectively, and the same applies to LRL^s and LRL^l. It is apparent that the closed region Ω is bounded by the RLR^s- and LRL^s-paths.

Denote by ℓ^s_{LRL}, ℓ^l_{LRL}, ℓ^s_{RLR}, and ℓ^l_{RLR} the lengths of LRL^s-, LRL^l-, RLR^s-, and RLR^l-paths from X to Y, respectively. Accordingly, we denote by ℓ_{RSR}, ℓ_{RSL}, ℓ_{LSR}, and ℓ_{LSL} the lengths of RSR-, RSL-, LSR-, and LSL-paths from X to Y, respectively. Once RSR-path does not exist, we set $\ell_{RSR} = +\infty$, and the same applies to ℓ_{RSL}, ℓ_{LSR}, ℓ_{LSL}, ℓ^s_{LRL}, ℓ^l_{LRL}, ℓ^s_{RLR}, and ℓ^l_{RLR}, accordingly. When $(X, Y) \in \mathcal{O}^c$ so that

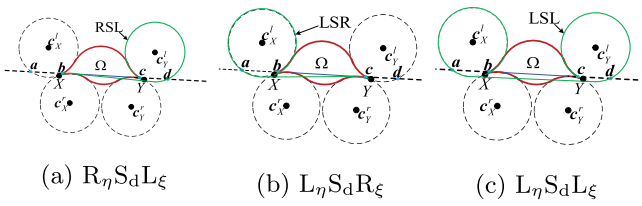

(a) $R_\eta S_d L_\xi$ (b) $L_\eta S_d R_\xi$ (c) $L_\eta S_d L_\xi$

Fig. 7. The CSC-paths with the existence of Ω.

the closed region Ω exists, we set

$$\ell_1 := \max\{\ell^s_{LRL},\ \ell^s_{RLR}\}$$
$$\ell_2 := \min \begin{Bmatrix} \ell_m + 2\pi,\ \ell^l_{LRL},\ \ell^l_{RLR}, \{\ell_{RSR}, \\ \ell_{RSL}, \ell_{LSR}, \ell_{LSL}\} \setminus \{\ell_m\} \end{Bmatrix} \quad (1)$$

Given any $(X, Y) \in \mathcal{O}^c$, the lengths of all the CSC- and CCC-paths, once they exist, can be computed by geometric analysis (Dubins, 1957; Shkel & Lumelsky, 2001). Thus, both ℓ_1 and ℓ_2 in Eq. (1) can be readily obtained. According to Yao et al. (2017, Proposition 1), we have $\ell_m < \ell_1$. By the following lemma, we shall show that $\ell_1 < \ell_2$ when the closed region Ω exists.

Lemma 3. *If $(X, Y) \in \mathcal{O}^c$, we have $\ell_1 < \ell_2$.*

Proof. By definition, for every $C_\eta C_\xi C_\zeta$-path related to ℓ^s_{RLR} and ℓ^s_{LRL}, the middle circular arc is a minor arc, i.e., $\xi < \pi$. According to Patsko et al. (2003, Lemma 2), once the closed region Ω exists, the sum of the other two circular arcs is less than the middle circular arc, i.e., $\eta + \zeta < \xi$. Thus, we have $\ell_1 = \eta + \xi + \zeta < 2\pi$, indicating $\ell_1 < \ell_m + 2\pi$. Thus, if $\ell_2 = \ell_m + 2\pi$, we have this lemma holds.

If $\ell_2 = \ell^l_{LRL}$ or ℓ^l_{RLR}, we immediately have $\ell_1 < \ell_2$ by the definitions of ℓ^s_{RLR}, ℓ^s_{LRL}, ℓ^l_{RLR}, and ℓ^l_{LRL}. Thus, if $\ell_2 = \ell^l_{LRL}$ or ℓ^l_{RLR}, we have this lemma holds.

From now on, we consider $\ell_2 \in \{\ell_{RSR}, \ell_{RSL}, \ell_{LSR}, \ell_{LSL}\} \setminus \{\ell_m\}$. Without loss of generality, let us assume $\ell_{RSR} \neq \ell_m$, i.e., ℓ_{RSR} is an element of $\{\ell_{RSR}, \ell_{RSL}, \ell_{LSR}, \ell_{LSL}\} \setminus \{\ell_m\}$. Then, we have that the RSR-path has intersections with the boundary of Ω. As a result, we have that ℓ_{RSR} is greater than $\min\{\ell^l_{RLR}, R^l_{LRL}\}$ according to Yao et al. (2017, Lemma 10). The same applies to other CSC-paths with its length in $\{\ell_{RSR}, \ell_{RSL}, \ell_{LSR}, \ell_{LSL}\} \setminus \{\ell_m\}$. Thus, if $\ell_2 \in \{\ell_{RSR}, \ell_{RSL}, \ell_{LSR}, \ell_{LSL}\} \setminus \{\ell_m\}$, we have $\ell_1 < \ell_2$, completing the proof. □

Lemma 4. *If $(X, Y) \in \mathcal{O}^c$, each CSC-path, with its length in $\{\ell_{RSR}, \ell_{RSL}, \ell_{LSR}, \ell_{LSL}\} \setminus \{\ell_m\}$, has anti-parallel tangents.*

Proof. Without loss of generality, let us assume that the shortest curvature-bounded path related to ℓ_m is of type RSR. Take the picture in Fig. 7 as an example. The extension of the straight-line segment of the RSR-path has four points intersecting with the circles C^l_X and C^l_Y, as shown by $\boldsymbol{a}$, $\boldsymbol{b}$, $\boldsymbol{c}$, and $\boldsymbol{d}$ in Fig. 7. Because of the existence of the closed region Ω, we have that the arcs $\widehat{\boldsymbol{axb}}$ and $\widehat{\boldsymbol{cyd}}$ are minor arcs. Regarding the RSL-path, we have that the switching point from S to L lies on the arc $\widehat{\boldsymbol{cyd}}$ (see Fig. 7(a)), indicating that the left-turn arc along the RSL-path is a major arc. As for the LSR-path, we have that the switching point from L to S lies on the arc $\widehat{\boldsymbol{axb}}$ (see Fig. 7(b)), indicating that the left-turn arc along the LSR-path is a major arc. As for the LSL-path, we have that the switching point from L to S and the switching point from S to L lie on $\widehat{\boldsymbol{cyd}}$ and $\widehat{\boldsymbol{axb}}$, respectively, as shown by Fig. 7(c), indicating that both left-turn arcs are major arcs. Therefore, if the RSR-path is the shortest curvature-bounded path, we have that at least one circular arc on each of the RSL-, LSR-, and LSL-paths is

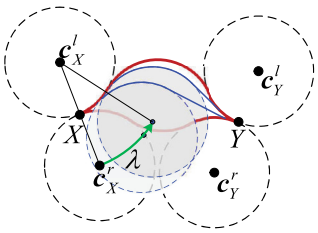

Fig. 8. Elongation of γ_m for $(X, Y) \in \mathcal{O}^c$.

a major arc, implying that all the RSL-, LSR-, and LSL-paths have anti-parallel tangents.

Analogously, we can prove by the same way that if one of the RSL-, LSR-, and LSL-paths is the shortest curvature-bounded path, then each other CSC-path with its length in $\{\ell_{\text{RSR}}, \ell_{\text{RSL}}, \ell_{\text{LSR}}, \ell_{\text{LSL}}\} \setminus \{\ell_m\}$ has anti-parallel tangents, completing the proof. □

Proposition 3. *If $(X, Y) \in \mathcal{O}^c$, for any $s \in [\ell_m, \ell_1] \cup [\ell_2, +\infty)$ there exists a $\gamma \in \Gamma(X, Y)$ so that $\ell(\gamma) = s$.*

Proof. We first consider the case that $s \in [\ell_m, \ell_1]$. Let us consider to move a circular disk of radius $1/\kappa$ to deform γ_m, as shown in Fig. 8. By changing the value of λ, we can see that γ_m can be elongated continuously from ℓ_m to ℓ_1. Thus, for any $s \in [\ell_m, \ell_1]$ there exists a $\gamma \in \Gamma(X, Y)$ so that $s = \ell(\gamma)$.

From now on, we consider the case of $s \in [\ell_2, +\infty)$. If $\ell_2 \in \{\ell^l_{\text{RLR}}, \ell^l_{\text{LRL}}\}$, then we have that the CCC-path with length of ℓ_2 has anti-parallel tangents according to the definitions of RLR^l and LRL^l in Fig. 6. Thus, if $\ell_2 \in \{\ell^l_{\text{RLR}}, \ell^l_{\text{LRL}}\}$, the CCC-path with length of ℓ_2 can be elongated to arbitrary length. If $\ell_2 = \ell_m + 2\pi$, we have that the path has anti-parallel tangents. If $\ell_2 \in \{\ell_{\text{RSR}}, \ell_{\text{RSL}}, \ell_{\text{LSR}}, \ell_{\text{LSL}}\} \setminus \{\ell_m\}$, we have that the path related to ℓ_2 has anti-parallel tangents, according to Lemma 4. Therefore, the path related to ℓ_2 can be elongated to arbitrary length, completing the proof. □

Proposition 3 indicates that for any $s \in [\ell_m, \ell_1] \cup [\ell_2, +\infty)$, we can find a $\gamma \in \Gamma(X, Y)$ so that $s = \ell(\gamma)$. From now on, we will prove that for any $s \in (\ell_1, \ell_2)$ it is impossible to find a $\gamma \in \Gamma(X, Y)$ so that $s = \ell(\gamma)$.

Before proceeding, we present some useful notations. Denote by $\mathcal{R}_{\boldsymbol{w}}(s) \subset \mathbb{R}^2$ the set that can be reached by all the curvature-bounded paths of length s, starting from X and ending with the final tangent vector being $\boldsymbol{w}$, i.e.,

$$\mathcal{R}_{\boldsymbol{w}}(s) := \{\boldsymbol{z} \in \mathbb{R}^2 | \ell(\gamma) = s \text{ with } \gamma \in \Gamma(X, (\boldsymbol{z}, \boldsymbol{w}))\}.$$

Denote by $\partial\mathcal{R}_{\boldsymbol{w}}(s)$ the boundary of $\mathcal{R}_{\boldsymbol{w}}(s)$, and denote by $\text{Int}\mathcal{R}_{\boldsymbol{w}}(s)$ the interior of $\mathcal{R}_{\boldsymbol{w}}(s)$. Denote by $P^{\boldsymbol{w}}_{\text{RSR}}(s) \in \mathbb{R}^2$ the set of all the points that can be reached by RSR-path of length $s > 0$, starting from X and ending with the final tangent being $\boldsymbol{w}$. The same explanation applies to $P^{\boldsymbol{w}}_{\text{RSL}}(s)$, $P^{\boldsymbol{w}}_{\text{LSR}}(s)$, $P^{\boldsymbol{w}}_{\text{LSL}}(s)$, $P^{\boldsymbol{w}}_{\text{RLR}}(s)$, and $P^{\boldsymbol{w}}_{\text{LRL}}(s)$.

Lemma 5. *If $(X, Y) \in \mathcal{O}^c$, we have that*

(1) there exists a positive number $\delta > 0$ so that $\boldsymbol{y} \in \mathcal{R}_{\boldsymbol{w}}(\ell_1 - \varepsilon)$ for every $\varepsilon \in (0, \delta)$;
(2) $\boldsymbol{y} \notin \mathcal{R}_{\boldsymbol{w}}(\ell_1 + \varepsilon)$ for any sufficiently small $\varepsilon > 0$.

Proof. By the definition of ℓ_1 in Eq. (1), we have $\boldsymbol{y} \in \mathcal{R}_{\boldsymbol{w}}(\ell_1)$. According to Proposition 3, for any $s \in [\ell_m, \ell_1]$, there exists a $\gamma \in \Gamma(X, Y)$ with its length being s. Thus, we have $\boldsymbol{y} \in \mathcal{R}_{\boldsymbol{w}}(\ell_1 - \eta)$ for $\eta \in [0, \ell_1 - \ell_m]$. Since $\ell_1 - \ell_m > 0$ (cf. Yao et al. (2017, Proposition 1)), it follows that there exists $\delta > 0$ so that $\boldsymbol{y} \in \mathcal{R}_{\boldsymbol{w}}(\ell_1 - \varepsilon)$ for every $\varepsilon \in (0, \delta)$.

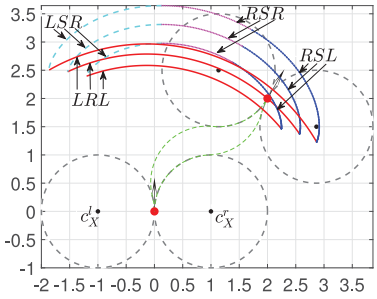

Fig. 9. Illustration of $\boldsymbol{y} \in P^{\boldsymbol{w}}_{\text{LRL}}(\ell_1) \subset \mathcal{R}_{\boldsymbol{w}}(\ell_1)$.

From now on, we proceed to proving $\boldsymbol{y} \notin \mathcal{R}_{\boldsymbol{w}}(\ell_1 + \varepsilon)$ for sufficiently small ε. Without loss of generality, let us assume that $\ell_1 = \ell^s_{\text{LRL}}$, i.e., the CCC-path with length of ℓ_1 from X to Y is of type LRL. In this case, according to Patsko and Fedotov (2020, 2022), we have that the set $P^{\boldsymbol{w}}_{\text{LRL}}(\ell_1)$ belongs to the boundary of $\mathcal{R}_{\boldsymbol{w}}(\ell_1)$, as shown by Fig. 9. Notice that $\boldsymbol{y} \in P^{\boldsymbol{w}}_{\text{LRL}}(\ell_1)$, indicating $\boldsymbol{y} \in \partial\mathcal{R}_{\boldsymbol{w}}(\ell_1)$.

Let $\mathcal{N}_\eta(\boldsymbol{y}) \subset \mathbb{R}^2$ be a circular neighborhood centered at Y with radius $\eta > 0$, i.e.,

$$\mathcal{N}_\eta(\boldsymbol{y}) := \{\boldsymbol{z} \in \mathbb{R}^2 | \|\boldsymbol{z} - \boldsymbol{y}\| \le \eta\}.$$

As $\boldsymbol{y} \in \partial\mathcal{R}_{\boldsymbol{w}}(\ell_1)$, we can choose a straight-line segment $\boldsymbol{p} : [0, 2\ell_1] \to \mathcal{N}_\eta(\boldsymbol{y})$ so that

- $\boldsymbol{p}(\ell_1) = \boldsymbol{y}$,
- $\boldsymbol{p}(t) \notin \mathcal{R}_{\boldsymbol{w}}(t)$ for $t \in [0, \ell_1)$, and
- $\boldsymbol{p}(t) \in \mathcal{R}_{\boldsymbol{w}}(t)$ for $t \in (\ell_1, 2\ell_1]$.

Let us consider a monotonically increasing sequence $(\varepsilon_i)_{i\in\mathbb{N}}$ so that $\varepsilon_0 = 0$ and $\varepsilon_i < 2\ell_1$ for $i \in \mathbb{N}$, and assume that there exists a large positive integer $N > 0$ so that $\varepsilon_N = \ell_1$. If $\eta > 0$ is small enough, for every ε_i, there exists a δ_i so that $\boldsymbol{p}(\varepsilon_i) \in P^{\boldsymbol{w}}_{\text{RLR}}(\ell_1 + \delta_i)$. Since the set $P^{\boldsymbol{w}}_{\text{RLR}}(\ell_1 + \delta_i)$ belongs to the boundary of $\mathcal{R}_{\boldsymbol{w}}(\ell_1 + \delta_i)$, it follows $\boldsymbol{p}(\varepsilon_i) \in \partial\mathcal{R}_{\boldsymbol{w}}(\ell_1 + \delta_i)$.

As the sequence (ε_i) is monotonically increasing, the direction of the straight line $\boldsymbol{p}$ can be chosen so that the sequence (δ_i) is monotonically increasing as well. Thus, picking an integer $\hat{i} \in \mathbb{N}$, we have $\boldsymbol{p}(\varepsilon_{\hat{i}+1}) \in \text{Int}\mathcal{R}_{\boldsymbol{w}}(\ell_1 + \delta_{\hat{i}})$ according to the first statement of this lemma. As $\boldsymbol{p}(\varepsilon_{\hat{i}}) \in \partial\mathcal{R}_{\boldsymbol{w}}(\ell_1 + \delta_{\hat{i}})$, it follows $\boldsymbol{p}(\varepsilon_{\hat{i}-1}) \notin \mathcal{R}_{\boldsymbol{w}}(\ell_1 + \delta_{\hat{i}})$. If $\hat{i} = N+1$, we then have $\boldsymbol{p}(\varepsilon_N) \notin \mathcal{R}_{\boldsymbol{w}}(\ell_1 + \delta_{N+1})$. Note that $\varepsilon_N = \ell_1$ and $\delta_N = 0$, indicating $\boldsymbol{y} = \boldsymbol{p}(\varepsilon_N) \notin \mathcal{R}_{\boldsymbol{w}}(\ell_1 + \delta_{N+1})$. If ε_{N+1} is close enough to ε_N, there exists $\delta > 0$ so that $\delta_{N+1} < \delta$, completing the proof. □

Lemma 6. *If $(X, Y) \in \mathcal{O}^c$, there exists $\delta > 0$ so that $\boldsymbol{y} \notin \mathcal{R}_{\boldsymbol{w}}(\ell_2 - \varepsilon)$ and $\boldsymbol{y} \in \mathcal{R}_{\boldsymbol{w}}(\ell_2 + \varepsilon)$ for every $\varepsilon \in (0, \delta)$.*

Proof. By the definition of ℓ_2 in Eq. (1), we have $\boldsymbol{y} \in \mathcal{R}_{\boldsymbol{w}}(\ell_2)$. According to Proposition 3, for any $s \in [\ell_2, +\infty)$ there exists a $\gamma \in \Gamma(X, Y)$ with its length being s. Thus, we have $\boldsymbol{y} \in \mathcal{R}_{\boldsymbol{w}}(\ell_2 + \eta)$ for any $\eta \ge 0$, indicating that there exists $\delta > 0$ so that $\boldsymbol{y} \in \mathcal{R}_{\boldsymbol{w}}(\ell_2 + \varepsilon)$ for every $\varepsilon \in (0, \delta)$.

From now on, we proceed to proving $\boldsymbol{y} \notin \mathcal{R}_{\boldsymbol{w}}(\ell_2 - \varepsilon)$ for sufficiently small $\varepsilon > 0$. By contradiction, let us assume that there exists a sufficiently small $\varepsilon > 0$ so that $\boldsymbol{y} \in \mathcal{R}_{\boldsymbol{w}}(\ell_2 - \varepsilon)$. Let us consider an object moving along a straight line $\boldsymbol{p} : [0, +\infty)$ so that at the instant ℓ_2 the object reaches the point $\boldsymbol{y}$, i.e., $\boldsymbol{p}(\ell_2) = \boldsymbol{y}$. Let $\mathcal{N}_\eta(\boldsymbol{y}) \subset \mathbb{R}^2$ be a circular neighborhood centered at Y with radius $\eta > 0$, i.e.,

$$\mathcal{N}_\eta(\boldsymbol{y}) := \{\boldsymbol{z} \in \mathbb{R}^2 | \|\boldsymbol{z} - \boldsymbol{y}\| \le \eta\}.$$

Without loss of generality, we consider $\ell_2 = \ell_{\text{RSR}}$ and $\ell_m = \ell_{\text{RSL}}$, i.e., the path associated with ℓ_2 is of type RSR and the shortest curvature-bounded path is of type RSL. Then, because the multi-valued set $P_{\text{LSR}}(t)$ for $t > 0$ is continuous (cf. Buzikov and Galyaev (2022, Lemma 6)), it follows that for any sufficiently small $\varepsilon > 0$ there exists $\eta > 0$ so that the length of LSR-path from X to a point in $\mathcal{N}_\eta(\boldsymbol{y})$ with the final tangent being $\boldsymbol{w}$ takes values in $(\ell_{\text{LSR}} - \varepsilon, \ell_{\text{LSR}} + \varepsilon)$. Without loss of generality, assume that the speed of the moving object is constant and small enough so that $\boldsymbol{p}(t) \in \mathcal{N}_\eta(\boldsymbol{y})$ for any $t \in [0, \ell_2]$. Then, for every $t \in [0, \ell_2]$, the LSR-path from X to the point $\boldsymbol{p}(t)$ with the final tangent being $\boldsymbol{w}$ has a length in $(\ell_{\text{LSR}} - \varepsilon, \ell_{\text{LSR}} + \varepsilon)$. By the definition of ℓ_2 in Eq. (1), we have $\ell_2 < \ell_{\text{LSR}}$. Therefore, if $\varepsilon > 0$ is small enough, the minimum time for a Dubins vehicle to intercept the moving object by following an LSR-path is greater than ℓ_2. Analogously, we can prove that the minimum time for a Dubins vehicle to intercept the moving object by following LSL-path or one of CCC-paths is greater than ℓ_2. Therefore, the minimum time for a Dubins vehicle from X to intercept the moving object with the final tangent being $\boldsymbol{w}$ by following a CSC- or a CCC-path is ℓ_2. This further indicates that the minimum time for a Dubins vehicle from X to intercept the moving object with the final tangent being $\boldsymbol{w}$ by following a curvature-bounded path is ℓ_2 (cf. Buzikov and Galyaev (2022, Theorem 7)). However, the contradicting assumption indicates that the minimum time for a Dubins vehicle from X to intercept the moving object with the final tangent being $\boldsymbol{w}$ by following a curvature-bounded path is less than ℓ_2. Hence, by contraposition, the proof is completed. □

As a result of Lemmas 5 and 6, we immediately obtain the following result.

Proposition 4. *If $(X, Y) \in \mathcal{O}^c$, for every $\gamma \in \Gamma(X, Y)$ we have $\ell(\gamma) \notin (\ell_1, \ell_2)$.*

Proof. By contradiction, let us assume that there exists an interval $[\hat{\ell}_1, \hat{\ell}_2] \subset (\ell_1, \ell_2)$ so that for any $\bar{\ell} \in [\hat{\ell}_1, \hat{\ell}_2]$ there exists a curvature-bounded path $\bar{\gamma} \in \Gamma(X, Y)$ with $\ell(\bar{\gamma}) = \bar{\ell}$. Then, according to Lemmas 5 and 6, there are at least three non-connected intervals in each of which we can establish a homotopy class of curvature-bounded paths. According to Ayala and Rubinstein (2016, Theorem 3.8), each homotopy class contains a minimal length path, whose geometric pattern is either CCC or CSC. Then, by the definitions of ℓ_1 and ℓ_2 in Eq. (1) as well as by Lemma 3, we have that the length of any CSC/CCC path is not in (ℓ_1, ℓ_2). This contradicts with the assumption. Hence, by contraposition, the proof is completed. □

This proposition indicates that if $(X, Y) \in \mathcal{O}^c$, γ_m cannot be elongated to arbitrary length. According to Propositions 1–4, we eventually have the main result summarized below.

Theorem 1. *Given any two X and Y so that $X \neq Y$, the following statements hold:*

(1) If $(X, Y) \notin \mathcal{O} \cup \mathcal{O}^c$, for every $s \geq \ell_m$ there exists a $\gamma \in \Gamma(X, Y)$ so that $\ell(\gamma) = s$.
(2) If $(X, Y) \in \mathcal{O}$, for every $s \geq \ell_m$ there exists a $\gamma \in \Gamma(X, Y)$ so that $\ell(\gamma) = s$.
(3) If $(X, Y) \in \mathcal{O}^c$, we have that (a) for every $s \in [\ell_m, \ell_1] \cup [\ell_2, +\infty)$ there exists a $\gamma \in \Gamma(X, Y)$ so that $\ell(\gamma) = s$; and (b) for every $\gamma \in \Gamma(X, Y)$ we have $\ell(\gamma) \notin (\ell_1, \ell_2)$.

This theorem gives the necessary and sufficient conditions for the existence of curvature-bounded path with an expected length. Given any X and Y in $T\mathbb{R}^2$, γ_m can be analytically obtained, indicating that the satisfactions of $(X, Y) \in \mathcal{O}$ and $(X, Y) \in \mathcal{O}^c$ can be readily checked. In addition, the values of ℓ_1 and ℓ_2, once they exist, can be computed analytically as well according to Shkel and Lumelsky (2001). Therefore, all the conditions in Theorem 1 are numerically or analytically verifiable, allowing one to predict the existence of curvature-bounded paths in $\Gamma(X, Y)$ with an expected length. Once the existence conditions are met, the elongation strategies proposed in the paper can be used to get a curvature-bounded path with the expected length.

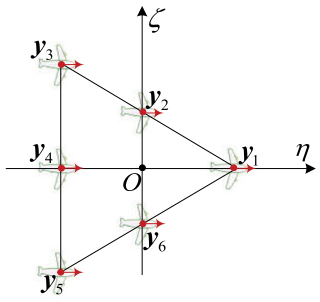

Fig. 10. Final positions of the six Dubins vehicles.

4. Numerical examples

In this section, some examples of minimum-time path planning for multiple Dubins vehicles to simultaneously achieve a triangle-shaped formation will be presented to illustrate the developments of the paper.

We consider that there are 6 Dubins vehicles, and the final position of Dubins vehicle #i is denoted by $\boldsymbol{y}_i$ $(i = 1, 2, \ldots, 6)$. Set the values of $\boldsymbol{y}_i$'s as $\boldsymbol{y}_1 = (\sqrt{3}, 0)$, $\boldsymbol{y}_2 = (0, 1)$, $\boldsymbol{y}_3 = (-\sqrt{3}, 2)$, $\boldsymbol{y}_4 = (-\sqrt{3}, 0)$, $\boldsymbol{y}_5 = (-\sqrt{3}, -2)$, and $\boldsymbol{y}_6 = (0, -1)$. Let the final tangent vectors of all the Dubins vehicles be the same and collinear with the η axis of the $O\eta\zeta$ frame, as shown in Fig. 10. It is clear from Fig. 10 that an equilateral-triangle formation will be formed if the six Dubins vehicles arrive their final conditions simultaneously.

Denote by $\boldsymbol{x}_i \in \mathbb{R}^2$ the initial position of Dubins vehicle #i, and let $\theta_i \in [0, 2\pi)$ be the angle between the initial tangent vector and the η axis, measured counterclockwise. The values of $\boldsymbol{x}_i$'s and θ_i's are generated randomly by uniform distribution for three different cases, and they are presented in Table 1.

Note that the initial tangent vector for Dubins vehicle #i is given by $\boldsymbol{v}_i := (\cos\theta_i, \sin\theta_i)$, and the final tangent vectors for all the six Dubins vehicles are the same as $\boldsymbol{w} = (1, 0)$. We denote by ℓ_m^i the length of the shortest curvature-bounded path for Dubins vehicle #i from the initial oriented point $(\boldsymbol{x}_i, \boldsymbol{v}_i)$ to the final oriented point $(\boldsymbol{y}_i, \boldsymbol{w})$. Accordingly, we denote by ℓ_1^i and ℓ_2^i the lengths corresponding to ℓ_1 and ℓ_2 defined in Eq. (1) for Dubins vehicle #i. In the case of $((\boldsymbol{x}_i, \boldsymbol{v}_i), (\boldsymbol{y}_i, \boldsymbol{w})) \in \mathcal{O}^c$, there exists a curvature-bounded path from $(\boldsymbol{x}_i, \boldsymbol{v}_i)$ to $(\boldsymbol{y}_i, \boldsymbol{w})$ if and only if its length lies in $[\ell_m^i, \ell_1^i] \cup [\ell_2^i, +\infty)$. The values of ℓ_m^i's, ℓ_1^i's, and ℓ_2^i's for cases A, B, and C are presented in Table 2.

Set

$$\Phi_i := \begin{cases} [\ell_m^i, \ell_1^i] \cup [\ell_2^i, +\infty) & \text{if } \ell_1^i < +\infty \text{ and } \ell_2^i < +\infty \\ [\ell_m^i, +\infty) & \text{if } \ell_1^i = +\infty \text{ and } \ell_2^i = +\infty \end{cases}$$

Then, according to Theorem 1, we have that the minimum time for the six Dubins vehicles to realize the triangle-shaped formation in Fig. 10 is given by

$$t_m := \min\{\Phi_1 \cap \Phi_2 \cap \Phi_3 \cap \Phi_4 \cap \Phi_5 \cap \Phi_6\} \tag{2}$$

Combining Eq. (2) and the data in Table 2, we have that the minimum time to realize the triangle-shaped formation is 9.7219, 8.7279, and 8.0845 for cases A, B, and C, respectively.

Table 1
The values of $(\boldsymbol{x}_i, \theta_i)$ for cases A, B, and C.

Item	Case A	Case B	Case C
1	(3.5313, −0.8619, 0.5305)	(4.3627, −1.0457, 6.0141)	(1.8829, 4.4956, 0.7477)
2	(1.2238, 0.9698, 4.8689)	(−2.3376, 0.2700, 0.2919)	(−0.9264, 0.0596, 3.1313)
3	(−3.5775, 1.3472, 1.6328)	(2.1806, 3.3248, 5.0283)	(−3.1202, 1.1104, 6.0302)
4	(1.6878, 0.9028, 2.5119)	(−0.8038, 3.4410, 0.8915)	(−4.4641, 1.4021, 0.5136)
5	(2.9336, 0.0854, 5.4582)	(−4.5537, −1.3816, 2.6500)	(1.6253, −3.9714, 3.9600)
6	(1.1577, −0.0281, 5.1353)	(1.5350, −0.2869, 5.7537)	(−0.7889, −2.7028, 1.4063)

Table 2
The values of ℓ_m^i's, ℓ_1^i's, and ℓ_2^i's for cases A, B, and C.

Item	ℓ_m^1	ℓ_1^1	ℓ_2^1	ℓ_m^2	ℓ_1^2	ℓ_2^2	ℓ_m^3	ℓ_1^3	ℓ_2^3	ℓ_m^4	ℓ_1^4	ℓ_2^4	ℓ_m^5	ℓ_1^5	ℓ_2^5	ℓ_m^6	ℓ_1^6	ℓ_2^6
Case A	7.3871	$+\infty$	$+\infty$	5.7164	$+\infty$	$+\infty$	7.0162	$+\infty$	$+\infty$	6.7435	$+\infty$	$+\infty$	9.7219	$+\infty$	$+\infty$	6.7160	$+\infty$	$+\infty$
Case B	8.5854	$+\infty$	$+\infty$	2.4540	2.7219	8.7279	8.6103	$+\infty$	$+\infty$	8.4646	$+\infty$	$+\infty$	6.3674	$+\infty$	$+\infty$	7.0891	$+\infty$	$+\infty$
Case C	8.0845	$+\infty$	$+\infty$	5.9104	$+\infty$	$+\infty$	7.8796	$+\infty$	$+\infty$	3.3402	3.6783	7.8609	6.6030	$+\infty$	$+\infty$	7.6161	$+\infty$	$+\infty$

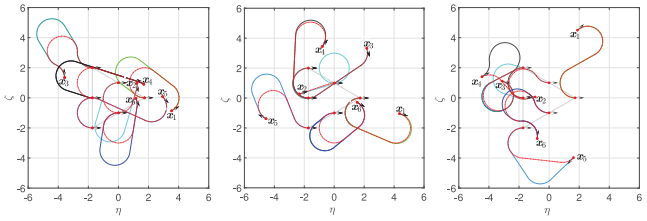

(a) Case A (b) Case B (c) Case C

Fig. 11. Cooperative paths for six Dubins vehicles to achieve a triangle-shaped formation.

Regarding case A, we can see from the data in Table 2 that in order to realize the minimum-time formation, we have to elongate the shortest curvature-bounded paths for Dubins vehicles #1, #2, #3, #4, and #6 to the length of 9.7219. The elongation strategies introduced in the paper can be used to elongate the shortest curvature-bounded paths, and the elongated paths are presented by the solid curves in Fig. 11(a), where the dashed curves denote the shortest curvature-bounded paths. If each Dubins vehicle follows its elongated path, all the six Dubins vehicles will simultaneously achieve the triangle-shaped formation in a minimum time.

Regarding case B, we can see from the data in Table 2 that in order to realize the minimum-time formation, we have to elongate the shortest curvature-bounded paths for Dubins vehicles #1, #3, #4, #5, and #6 to the length of 8.7279. Note that Dubins vehicle #2 follows a CSC-path with length of ℓ_2 instead of the shortest curvature-bounded path. The elongated path of each Dubins vehicle for the minimum-time formation is presented by the solid curve in Fig. 11(b).

For case C, the paths of all the six Dubins vehicles have to be elongated to the length of 8.0845 in order to realize the minimum-time operation of simultaneously achieving their final conditions, required for the triangle-shaped formation. Since $\ell_2^4 < 8.0845$, it follows that the shortest curvature-bounded path for Dubins vehicle #4 cannot be elongated to 8.0845 according to Theorem 1. We can get a curvature-bounded path with length of 8.0845 by elongating from the CCC-path of length $\ell_2^4 = 7.8609$, as shown by the solid curve starting from $\boldsymbol{x}_4$ in Fig. 11(c).

5. Conclusions

It was shown in the paper that, if the shortest curvature-bounded path between two oriented points takes a geometric pattern of CCC, it can be elongated to arbitrary length. If the shortest curvature-bounded path between two oriented points takes a geometric pattern of CSC, the space of pairs of initial/final oriented points was divided into two subspaces $\mathcal{O}$ and $\mathcal{O}^c$. If the space of pairs of initial/final oriented points lies in $\mathcal{O}$, the shortest curvature-bounded path can be elongated to arbitrary length. However, if the space of pairs of initial/final oriented points lies in $\mathcal{O}^c$, there exists an interval so that between the two oriented points there is no curvature-bounded path with its length in the interval. In addition, the boundary values of the non-existence interval were presented. As a result, given any two oriented points and any expected length, it can be readily checked if there exists a curvature-bounded path with the expected length; once it exists, an elongation strategy was provided. All the developments were finally demonstrated and verified by three examples of cooperative path planning for multiple Dubins vehicles to realize a triangle-shaped formation.

References

Ayala, José (2015). Length minimising bounded curvature paths in homotopy classes. *Topology and its Applications*, *193*, 140–151.

Ayala, José (2017). On the topology of the spaces of curvature constrained plane curves. *Advances in Geometry*, *17*(3), 283–292.

Ayala, José, & Rubinstein, Hyam (2014). Non-uniqueness of the homotopy class of bounded curvature paths. arXiv.

Ayala, José, & Rubinstein, Hyam (2016). The classification of homotopy classes of bounded curvature paths. *Israel Journal of Mathematics*, *213*, 79–107.

Bakolas, Efstathios, & Tsiotras, Panagiotis (2013). Optimal synthesis of the Zermelo–Markov–Dubins problem in a constant drift field. *Journal of Optimization Theory and Applications*, *156*(2), 469–492.

Boissonnat, Jean-Daniel, Cérézo, André, & Leblond, Juliette (1994). Shortest paths of bounded curvature in the plane. *Journal of Intelligent and Robotic Systems*, *11*(1), 5–20.

Bui, Xuan-Nam, Boissonnat, Jean-Daniel, Souères, Philippe, & Laumond, Jean-Paul (1994). Shortest path synthesis for Dubins non-holonomic robot. In *Proceedings of the 1994 IEEE international conference on robotics and automation, Vol. 1* (pp. 2–7).

Buzikov, Maksim E., & Galyaev, Andrey A. (2022). Minimum-time lateral interception of a moving target by a Dubins car. *Automatica*, *135*, Article 109968.

Ding, Yulong, Xin, Bin, & Chen, Jie (2019). Curvature-constrained path elongation with expected length for Dubins vehicle. *Automatica*, *108*, Article 108495.

Dubins, Lester E. (1957). On curves of minimal length with a constraint on average curvature, and with prescribed initial and terminal positions and tangents. *American Journal of Mathematics*, *79*(3), 497–516.

Kaya, C. Yalçın (2017). Markov–Dubins path via optimal control theory. *Computational Optimization and Applications*, *68*(3), 719–747.

Markov, Andrey Andreyevich (1887). Some examples of the solution of a special kind of problem on greatest and least quantities. *Soobscenija Charkovskogo Matematiceskogo Obscestva*, *1*, 250–276.

Meyer, Yizhaq, Isaiah, Pantelis, & Shima, Tal (2015). On Dubins paths to intercept a moving target. *Automatica*, *53*, 256–263.

Ortiz, Andres, Kingston, Derek, & Langbort, Cédric (2013). Multi-UAV velocity and trajectory scheduling strategies for target classification by a single human operator. *Journal of Intelligent and Robotic Systems*, *70*(1), 255–274.
Patsko, Valerii S., & Fedotov, Andrey A. (2020). Analytic description of a reachable set for the Dubins car. *Trudy Instituta Matematiki i Mekhaniki URO RAN*, *26*(1), 182–197.
Patsko, Valerii, & Fedotov, Andrey (2022). Three-dimensional reachable set for the Dubins car: Foundation of analytical description. *Communications in Optimization Theory*, 1–42.
Patsko, Valerii S., Pyatko, S. G., & Fedotov, Andrey A. (2003). Three-dimensional reachability set for a nonlinear control system. *Journal of Computer and Systems Sciences International*, *42*(3), 320–328.
Schumacher, Corey, Chandler, Phillip, Rasmussen, Steven, & Walker, David (2003). Path elongation for UAV task assignment. In *AIAA guidance, navigation, and control conference and exhibit* (p. 5585).
Shanmugavel, Madhavan, Tsourdos, Antonios, White, Brian, & Żbikowski, Rafał (2010). Co-operative path planning of multiple UAVs using Dubins paths with clothoid arcs. *Control Engineering Practice*, *18*(9), 1084–1092.
Shanmugavel, Madhavan, Tsourdos, Antonios, Zbikowski, Rafal, & White, Brian (2005). Path planning of multiple UAVs using Dubins sets. In *AIAA guidance, navigation, and control conference and exhibit* (p. 5827).
Shkel, Andrei M., & Lumelsky, Vladimir (2001). Classification of the Dubins set. *Robotics and Autonomous Systems*, *34*(4), 179–202.
Yao, Weiran, Qi, Naiming, Yue, Chengfei, & Wan, Neng (2020). Curvature-bounded lengthening and shortening for restricted vehicle path planning. *IEEE Transactions on Automation Science and Engineering*, *17*(1), 15–28.
Yao, Weiran, Qi, Naiming, Zhao, Jun, & Wan, Neng (2017). Bounded curvature path planning with expected length for Dubins vehicle entering target manifold. *Robotics and Autonomous Systems*, *97*, 217–229.
Yao, Weiran, Xin, Liming, Peng, Yan, Chen, Yang, Qi, Naiming, & Sun, Yu (2020). Trajectory consensus for coordination of multiple curvature-bounded vehicles. *IEEE Transactions on Cybernetics*, 1–13.

Zheng Chen received the Ph.D. degree in Applied Mathematics from the University Paris-Saclay in 2016, the M.Sc. and B.Sc. in Aerospace Engineering from Northwestern Polytechnical University in 2013 and 2010, respectively. He is currently a professor with the School of Aeronautics and Astronautics at Zhejiang University. His current research interests revolve around real-time optimal control and nonlinear optimal guidance in aerospace engineering.

Kun Wang received the B.Sc. degree in Materials Science and Engineering from Shandong University in 2017, and the M.Sc. degree in Aerospace Engineering from Nanjing University of Aeronautics and Astronautics in 2020. He is currently pursuing his Ph.D. degree from the School of Aeronautics and Astronautics at Zhejiang University. His current research interests include optimal guidance and control for autonomous vehicles.

Heng Shi received the Ph.D. degree in Computer Science from Tsinghua University in 2020, the M.Sc. and B.Sc. in Aerospace Engineering from Beihang University in 2012 and 2015, respectively. He is currently an assistant research fellow with the Department of Precision Instrument at Tsinghua University. His current research interests include cooperative guidance, intelligent control and unmanned systems.